Inorganic Chemistry

Article

pubs.acs.org/IC

New Bismuth Selenium Oxides: Syntheses, Structures, and Characterizations of Centrosymmetric $Bi_2(SeO_3)_2(SeO_4)$ and $Bi_2(TeO_3)_2(SeO_4)$ and Noncentrosymmetric $Bi(SeO_3)(HSeO_3)$

Eun Pyo Lee,[†] Seung Yoon Song,[†] Dong Woo Lee, and Kang Min Ok*

Department of Chemistry, Chung-Ang University, 221 Heukseok-dong, Dongjak-gu, Seoul 156-756, Republic of Korea

Supporting Information

ABSTRACT: Three new mixed metal selenium oxides materials, $Bi_2(SeO_3)_2(SeO_4)$, $Bi_2(TeO_3)_2(SeO_4)$, and $Bi(SeO_3)(HSeO_3)$, have been synthesized by hydrothermal and solid-state reactions using $Bi(NO_3)_3{\cdot}5H_2O$, SeO_2 (or TeO_2), H_2SeO_4, and Bi_2O_3 as reagents. The reported materials have been structurally characterized by single crystal X-ray diffraction. While $Bi_2(SeO_3)_2(SeO_4)$ and $Bi_2(TeO_3)_2(SeO_4)$ are crystallographically centrosymmetric (CS), $Bi(SeO_3)(HSeO_3)$ crystallizes in a noncentrosymmetric (NCS) space group. The isostructural $Bi_2(SeO_3)_2(SeO_4)$ and $Bi_2(TeO_3)_2(SeO_4)$ exhibit three-dimensional framework structures that are composed of BiO_6, $Se^{4+}O_3$ (or $Te^{4+}O_3$), and $Se^{6+}O_4$ polyhedra. However, $Bi(SeO_3)(HSeO_3)$ exhibits corrugated layers that are composed of BiO_5, $Se^{4+}O_3$, and $Se^{4+}O_2(OH)$ polyhedra. All three materials contain local asymmetric coordination environments attributable to the lone pairs on the Bi^{3+}, Se^{4+}, and/or Te^{4+} cations. Powder second-harmonic generation (SHG) measurements on NCS $Bi(SeO_3)(HSeO_3)$ using 1064 nm radiation indicate that the material has a SHG efficiency of approximately 20 times that of α-SiO_2 and is not phase-matchable (type 1). The origin and magnitude of the SHG efficiency of $Bi(SeO_3)(HSeO_3)$ is explained by determining the net direction of the polarizations arising from individual asymmetric polyhedra. Infrared spectroscopy, thermal analysis, elemental analysis, and dipole moment calculations for the reported materials are also presented.

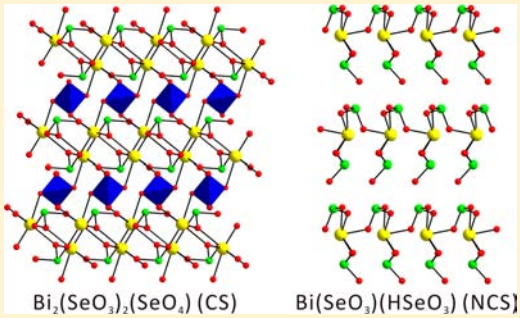

INTRODUCTION

Metal oxides accommodating lone pair cations such as Pb^{2+}, Bi^{3+}, Te^{4+}, and I^{5+} have been of great interest attributable to their rich structural chemistry.[1] In virtue of their variable coordination environments, materials composed of lone pair cations often exhibit certain flexible structural backbones.[2] In addition, once the variable geometry of the lone pair cations is amalgamated with a variety of polyhedra of transition metal cations and/or halides, a great deal of framework architectures would be expected. Especially with the transition metal oxyhalides materials, the lone pair cations play a role as chemical scissors: while the more chalcophilic lone pair cations have a tendency to make bonds with oxygen, the late transition metal cations are connected to halogen.[3] That separation of the chalcophile and halophile results in materials with low-dimensional structures such as chains and layers. Meanwhile, quite a lot of materials with lone pair cations have demonstrated technologically important properties such as second-harmonic generation (SHG), piezoelectricity, pyroelectricity, and ferroelectricity.[4] The aforementioned functional properties are, in fact, observed from noncentrosymmetric (NCS) materials, i.e., compounds crystallizing in a space group with no center of symmetry. The crystallographic NCS may have been achieved with ease from compounds containing lone pair cations because of their asymmetric coordination environment.[5] The lone pairs are thought to be the result of a second-order Jahn–Teller (SOJT) distortions,[6] which reduces the energy between the highest occupied s orbital and the lowest unoccupied p orbital through s–p mixing.[7] We have focused on discovering new oxides materials by combining different lone pair cations, from which extraordinary structural architectures as well as remarkable properties could be expected. More specifically, we have been very interested in Bi^{3+}–Se^{4+} (or Te^{4+})–oxide system, in which the constituting cations inherently possess asymmetric coordination geometries attributable to the nonbonded electron pairs. With respect to bismuth(III) selenium(IV) oxides, several materials with a variety of structural motifs, namely, $Bi_2Cu(SeO_3)_4$,[8] $(Bi_2O)Cu(SeO_3)_3(H_2O)$,[9] $Bi_2(SeO_3)_3$,[10] Bi_2SeO_5,[11] $Bi_2Mo_2Se_2O_{13}$,[12] and $Bi_2V_2Se_4O_{16}$[12] have been reported. Among them, $(Bi_2O)Cu(SeO_3)_3(H_2O)$[9] and Bi_2SeO_5[11] crystallize in NCS space groups. Moreover, while we were investigating the system, we happened to discover selenite–selenate compounds, i.e., materials containing both Se^{4+} and Se^{6+} cations through oxidation reactions. In fact, the mixed valent materials are of special interest, since much richer structural chemistry could be obtained attributable to the combination of asymmetric $Se^{4+}O_3$ polyhedra and $Se^{6+}O_4$ tetrahedra within the extended frameworks. Including the mineral schmiederit,

Received: January 30, 2013
Published: March 18, 2013

dx.doi.org/10.1021/ic4002384 | Inorg. Chem. 2013, 52, 4097–4103

$Pb_2Cu_2(OH)_3(SeO_3)(SeO_4)$,[13] several selenite−selenate mixed valent compounds with interesting structures have been reported.[14] In this Article, we present the syntheses, crystal structures, infrared spectra, thermogravimetric analyses, and dipole moment calculations on three new bismuth selenium oxides materials, $Bi_2(SeO_3)_2(SeO_4)$, $Bi_2(TeO_3)_2(SeO_4)$, and $Bi(SeO_3)(HSeO_3)$. With the NCS $Bi(SeO_3)(HSeO_3)$, we will also demonstrate how the net direction of polarizations is obtained from individual asymmetric polyhedra and how it influences the magnitude of the SHG efficiency.

EXPERIMENTAL SECTION

Reagents. $Bi(NO_3)_3{\cdot}5H_2O$ (Aldrich, 98%), Bi_2O_3 (Alfa Aesar, 99%), SeO_2 (Aldrich, 98%), TeO_2 (Acros, 98%), and H_2SeO_4 (Aldrich, 98%) were used as received.

Syntheses. $Bi_2(SeO_3)_2(SeO_4)$ and $Bi_2(TeO_3)_2(SeO_4)$ were prepared by hydrothermal reactions. For $Bi_2(SeO_3)_2(SeO_4)$, 0.970 g (2.00×10^{-3} mol) of $Bi(NO_3)_3{\cdot}5H_2O$, 0.222 g (2.00×10^{-3} mol) of SeO_2, 0.172 g (1.00×10^{-3} mol) of H_2SeO_4, and 2 mL of deionized water were combined. For $Bi_2(TeO_3)_2(SeO_4)$, 0.970 g (2.00×10^{-3} mol) of $Bi(NO_3)_3{\cdot}5H_2O$, 0.319 g (2.00×10^{-3} mol) of TeO_2, 0.172 g (1.00×10^{-3} mol) of H_2SeO_4, and 5 mL of deionized water were combined. The respective reaction mixtures were placed in 23 mL Teflon-lined stainless steel autoclaves. The autoclaves were subsequently sealed and heated to 230 °C to generate autogenous pressures, held for 4 days, and cooled at a rate of 6 °C h^{-1} to room temperature. After cooling, the autoclaves were opened, and the products were recovered by filtration and washed with distilled water. Pure samples that are composed of colorless crystals and white polycrystalline phases of $Bi_2(SeO_3)_2(SeO_4)$ and $Bi_2(TeO_3)_2(SeO_4)$ were obtained in 38% and 31% yields based on the bismuth nitrate.

Crystals of $Bi(SeO_3)(HSeO_3)$ were grown through a standard solid-state reaction. A 0.070 g (1.50×10^{-4} mol) portion of Bi_2O_3 and 0.399 g (3.60×10^{-3} mol) of SeO_2 were mixed with an agate mortar and pestle. The reaction mixture was exposed to vapor from boiling water for 30 s. A schematic diagram showing how water vapor was initially exposed to the reaction mixture is available as Supporting Information. Then, the mixture was introduced into a fused silica tube that was subsequently evacuated and sealed. The tube was gradually heated to 380 °C for 5 h, 600 °C for 24 h, and cooled at a rate of 6 °C h^{-1} to room temperature. The product contained colorless block shaped crystals of $Bi(SeO_3)(HSeO_3)$ with selenic acid and unknown amorphous phase. Although several attempts have been made, we found that it was difficult to prepare pure polycrystalline samples of $Bi(SeO_3)(HSeO_3)$ by combining stoichiometric amounts of reactants through the similar solid-state reactions. Thus, an excess amount of SeO_2 was used in the initial step. A 0.233 g (5.00×10^{-4} mol) portion of Bi_2O_3 and 0.444 g (4.00×10^{-3} mol) of SeO_2 were thoroughly mixed with an agate mortar and pestle. The reaction mixture was exposed to water vapor for 30 s and reground for 5 min. Then the mixture was introduced into a fused silica tube that was subsequently evacuated and sealed. The tube was gradually heated to 380 °C for 5 h, 600 °C for 24 h, and cooled at a rate of 60 °C h^{-1} to room temperature. The product was obtained as a mixture of polycrystalline $Bi(SeO_3)(HSeO_3)$ and H_2SeO_3. However, pure $Bi(SeO_3)(HSeO_3)$ was successfully isolated by filtration after washing with copious amount of deionized water because H_2SeO_3 is water-soluble. After filtration, polycrystalline $Bi(SeO_3)(HSeO_3)$ was dried in air for 24 h. The powder X-ray diffraction patterns on the resultant bulk samples of $Bi_2(SeO_3)_2(SeO_4)$, $Bi_2(TeO_3)_2(SeO_4)$, and $Bi(SeO_3)(HSeO_3)$ exhibited materials that were single phases and were in good agreement with the generated patterns from the single-crystal data (see the Supporting Information).

Single Crystal X-ray Diffraction. The structures of the reported materials were determined by a standard crystallographic method. A colorless block ($0.022 \times 0.032 \times 0.052$ mm^3) for $Bi_2(SeO_3)_2(SeO_4)$, a colorless block ($0.028 \times 0.034 \times 0.047$ mm^3) for $Bi_2(TeO_3)_2(SeO_4)$, and a colorless plate ($0.017 \times 0.034 \times 0.051$ mm^3) for $Bi(SeO_3)(HSeO_3)$ were used for single-crystal data analyses. All of the data were collected using a Bruker SMART BREEZE diffractometer equipped with a 1K CCD area detector using graphite monochromated Mo Kα radiation at 173 K. A hemisphere of data was collected using a narrow-frame method with scan widths of 0.30° in ω, and an exposure time of 5 s/frame. The first 50 frames were remeasured at the end of the data collection to monitor instrument and crystal stability. The maximum correction applied to the intensities was <1%. The data were integrated using the SAINT program,[15] with the intensities corrected for Lorentz factor, polarization, air absorption, and absorption attributable to the variation in the path length through the detector faceplate. A semiempirical absorption correction was made on the hemisphere of data with the SADABS program.[16] The data were solved and refined using SHELXS-97 and SHELXL-97, respectively.[17] All calculations were performed using the WinGX-98 crystallographic software package.[18] With $Bi(SeO_3)(HSeO_3)$, the orthorhombic metrics suggest a pseudomerohedral twinning of the crystal from Laue class $2/m$ to mmm. In fact, when we refined the structure in the orthorhombic space group $Cmc2_1$, oxygen atoms were disordered and resulted in an improbable coordination environment for Se^{4+}, i.e., SeO_5. However, the structure along with the twin ratio was successfully refined in the monoclinic space group Cc. Crystallographic data and selected bond distances for the reported materials are given in Table 1 and Supporting Information, respectively.

Table 1. Crystallographic Data for $Bi_2(SeO_3)_2(SeO_4)$, $Bi_2(TeO_3)_2(SeO_4)$, and $Bi(SeO_3)(HSeO_3)$

formula	$Bi_2Se_3O_{10}$	$Bi_2Te_2SeO_{10}$	$BiHSe_2O_6$
fw	814.84	912.12	463.91
space group	$I2/a$ (No. 15)	$I2/a$ (No. 15)	Cc (No. 9)
a (Å)	8.04400(10)	8.0995(2)	5.5407(4)
b (Å)	7.43770(10)	7.4835(2)	6.6746(4)
c (Å)	14.7456(2)	14.8219(5)	15.4756(12)
β (deg)	97.274(2)	97.824(3)	90.003(5)
V (Å^3)	875.11(2)	890.03(4)	572.32(7)
Z	4	4	4
T (K)	173.0(2)	173.0(2)	173.0(2)
λ (Å)	0.710 73	0.710 73	0.710 73
ρ_{calcd} (g cm^{-3})	6.184	6.807	5.384
μ (mm^{-1})	52.681	50.046	43.483
$R(F)^a$	0.0269	0.0470	0.0485
$R_w(F_o^2)^b$	0.0639	0.1312	0.1206

$^aR(F) = \Sigma||F_o| - |F_c||/\Sigma |F_o|$. $^bR_w(F_o^2) = [\Sigma w(F_o^2 - F_c^2)^2/\Sigma w(F_o^2)^2]^{1/2}$.

Powder X-ray Diffraction. Powder X-ray diffraction was used to confirm the phase purity of the synthesized materials. The powder XRD patterns were collected on a Bruker D8-Advance diffractometer using Cu Kα radiation at room temperature with 40 kV and 40 mA. The polycrystalline samples were mounted on sample holders and scanned in the 2θ range 5−70° with a step size of 0.02°, and a step time of 0.2 s. The experimental powder XRD patterns are in good agreements with the calculated data from the single-crystal models.

Infrared Spectroscopy. Infrared spectra were recorded on a Varian 1000 FT-IR spectrometer in the 400−4000 cm^{-1} range, with the samples embedded in KBr matrixes.

Thermogravimetric Analysis. Thermogravimetric analyses were performed on a Setaram LABSYS TG-DTA/DSC thermogravimetric analyzer. The polycrystalline samples were contained within alumina crucibles and heated at a rate of 10 °C min^{-1} from room temperature to 800 °C under flowing argon.

Scanning Electron Microscope/Energy Dispersive Analysis by X-ray (SEM/EDAX). SEM/EDAX analysis has been performed using a Hitachi S-3400N/Horiba Energy EX-250 instruments. EDAX for the reported materials exhibit the same Bi:Se (or Te) ratios as those obtained from X-ray single crystal diffraction analyses.

dx.doi.org/10.1021/ic4002384 | Inorg. Chem. 2013, 52, 4097−4103

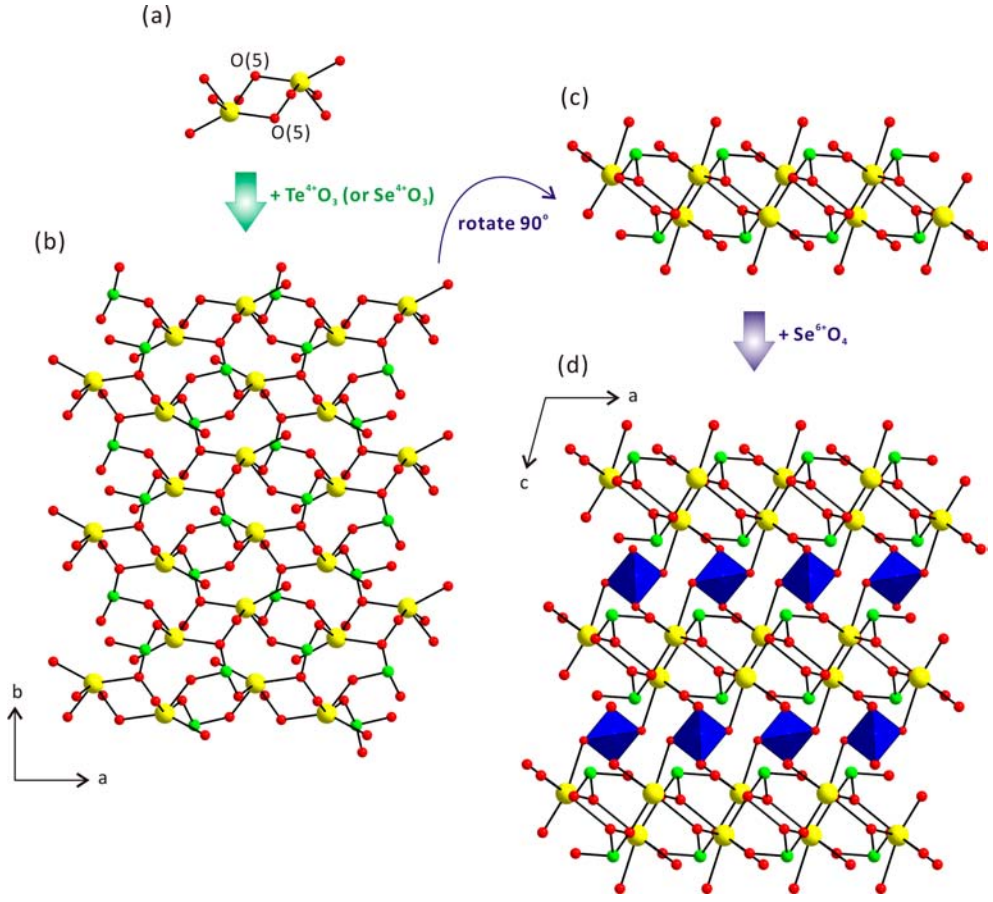

Figure 1. Ball-and stick and polyhedral models of $Bi_2(SeO_3)_2(SeO_4)$ representing (a) Bi_2O_{10} dimers consisting of two edge-shared BiO_6 polyhedra, (b) the linking of $Se^{4+}O_3$ or $Te^{4+}O_3$ polyhedra to form a layer in the *ab*-plane, (c) a layer in the *ac*-plane, and (d) the connection of $Se^{6+}O_4$ tetrahedra (green, Se^{4+}; blue, Se^{6+}; yellow, Bi^{3+}; red, O).

Second-Order Nonlinear Optical Measurements. Powder SHG measurements on NCS polycrystalline $Bi(SeO_3)(HSeO_3)$ were performed on a modified Kurtz-NLO system[19] using 1064 nm radiation. A DAWA Q-switched Nd:YAG laser, operating at 20 Hz, was used for the measurements. Because SHG efficiency has been shown to depend strongly on particle size, polycrystalline samples were ground and sieved (Newark Wire Cloth Co.) into distinct particle size ranges (20−45, 45−63, 63−75, 75−90, 90−125, >125 μm). To make relevant comparisons with known SHG materials, crystalline α-SiO_2 and $LiNbO_3$ were also ground and sieved into the same particle size ranges. Powders with particle size 45−63 μm were used for comparing SHG intensities. All the powder samples with different particle sizes were placed in separate capillary tubes. No index matching fluid was used in any of the experiments. The SHG light, i.e., 532 nm green light, was collected in reflection and detected by a photomultiplier tube (Hamamatsu). To detect only the SHG light, a 532 nm narrow-pass interference filter was attached to the tube. A digital oscilloscope (Tektronix TDS1032) was used to view the SHG signal. A detailed description of the equipment and the methodology used has been published.[20]

RESULTS AND DISCUSSION

Syntheses. Initial syntheses reactions using $Bi(NO_3)_3{\cdot}5H_2O$ and SeO_2 and/or TeO_2 under hydrothermal conditions resulted in the formation of $Bi_2(Se^{4+}O_3)_2(Se^{6+}O_4)$ and $Bi_2(Te^{4+}O_3)_2(Se^{6+}O_4)$. One can notice that some or all of the Se^{4+} cations have been oxidized to Se^{6+} during the hydrothermal reactions for the reported materials. It is well-known that nitrate ion in aqueous solution acts as an oxidizing agent.[21] We were able to prepare pure phases of $Bi_2(Se^{4+}O_3)_2(Se^{6+}O_4)$ and $Bi_2(Te^{4+}O_3)_2(Se^{6+}O_4)$ directly by introducing Se^{6+} source, i.e., H_2SeO_4, which confirms the oxidation states of Se^{6+} in the products and the oxidizing capability of $Bi(NO_3)_3{\cdot}5H_2O$.

Single crystals of $Bi(SeO_3)(HSeO_3)$ were initially obtained by a solid-state reaction in a sealed fused silica tube. It should be noted that SeO_2 is hygroscopic and easily forms H_2SeO_3 in the presence of water. Thus, we believe that a small amount of water was introduced during the mixing of starting materials under humid environment. Later, we were able to successfully isolate pure $Bi(SeO_3)(HSeO_3)$ by using wet SeO_2.

Structures. $Bi_2(SeO_3)_2(SeO_4)$ and $Bi_2(TeO_3)_2(SeO_4)$. $Bi_2(SeO_3)_2(SeO_4)$ and $Bi_2(TeO_3)_2(SeO_4)$ are isostructural and crystallize in the monoclinic space group $I2/a$ (No. 15). The structures of the materials are composed of $Bi^{3+}O_6$, $Se^{4+}O_3$ (or $Te^{4+}O_3$), and $Se^{6+}O_4$ polyhedra (see Figure 1). Within an asymmetric unit, Bi^{3+}, Se^{4+} (or Te^{4+}), and Se^{6+} cations exist. The Bi^{3+} cation is linked to six oxygen atoms and forms a distorted BiO_6 polyhedron. The Bi−O bond distances range from 2.201(6) to 2.734(7) Å for $Bi_2(SeO_3)_2(SeO_4)$ and from 2.211(14) to 2.666(17) Å for $Bi_2(TeO_3)_2(SeO_4)$. The O−Bi−O bond angles range from 66.8(3)° to 148.8(2)° for $Bi_2(SeO_3)_2(SeO_4)$ and from 65.3(6)° to 147.7(5)° for $Bi_2(TeO_3)_2(SeO_4)$. The unique Se^{4+} or Te^{4+} cation is connected to three oxygen atoms and exhibits an asymmetric coordination environment in $Se^{4+}O_3$ or $Te^{4+}O_3$ polyhedra attributable to the lone pairs. The Se^{4+}−O bond lengths and the O−Se^{4+}−O bond angles for $Bi_2(SeO_3)_2(SeO_4)$ range from

dx.doi.org/10.1021/ic4002384 | Inorg. Chem. 2013, 52, 4097−4103

1.687(6) to 1.742(7) Å and from 96.7(3)° to 105.3(3)°, respectively. Also, the Te^{4+}–O bond distances and the O–Te^{4+}–O bond angles for $Bi_2(TeO_3)_2(SeO_4)$ range from 1.800(14) to 1.846(14) Å and 92.7(7)° to 102.6(7)°, respectively. The Se^{4+} or Te^{4+} cations are in asymmetric coordination environments attributable to the stereoactive lone pair. The Se^{6+} cation is coordinated by four oxygen atoms and shows $Se^{6+}O_4$ tetrahedra. While the Se^{6+}–O bond lengths and the O–Se^{6+}–O bond angles for $Bi_2(SeO_3)_2(SeO_4)$ range from 1.630(7) to 1.646(7) Å and from 102.4(4)° to 114.0(6)°, respectively, those for $Bi_2(TeO_3)_2(SeO_4)$ range from 1.580(19) to 1.663(16) Å and 102.4(8)° to 116.6(13)°, respectively.

As seen in Figure 1a, two six-coordinate BiO_6 polyhedra share their edges through O(5) and form Bi_2O_{10} dimers. The Bi_2O_{10} dimers are further linked by $Se^{4+}O_3$ or $Te^{4+}O_3$ along the [001] and [00−1] directions through O(3), O(4), and O(5), which produces a layer in the *ab*-plane (see Figure 1b,c). While the lone pairs on the Bi^{3+} point approximately toward the [010] and [0−10] directions, those on the Se^{4+} or Te^{4+} point approximately toward the [001] and [00−1] directions. Each layer is further connected by $Se^{6+}O_4$ tetrahedra through O(1) and O(2) along the [001] direction and a three-dimensional framework structure is completed (see Figure 1d). In connectivity terms, the structure of $Bi_2(SeO_3)_2(SeO_4)$ and $Bi_2(TeO_3)_2(SeO_4)$ can be described as a neutral framework of $\{2[Bi^{3+}O_{4/2}O_{2/3}]^{-2.333}\ 2[Se^{4+}(or\ Te^{4+})O_{2/2}O_{1/3}]^{+1.333}[Se^{6+}O_{4/2}]^{+2}\}^0$. Bond valence calculations[22] for the Bi^{3+}, Se^{4+} (or Te^{4+}), Se^{6+}, and O^{2-} result in values in the ranges of 2.69–2.86, 3.98–4.29, 6.00–6.25, and 1.79–2.32, respectively.

$Bi(SeO_3)(HSeO_3)$. $Bi(SeO_3)(HSeO_3)$ crystallizes in the noncentrosymmetric space group *Cc* (No. 9). The material is a new bismuth selenite exhibiting a layered structure that is composed of BiO_5, SeO_3, and $SeO_2(OH)$ polyhedra (see Figure 2). Within an asymmetric unit, a unique Bi^{3+} and two Se^{4+} cations exist. The Bi^{3+} cations are connected to five oxygen atoms and form distorted BiO_5 square pyramids. The BiO_5 polyhedra are in asymmetric coordination environments attributable to the lone pairs. The Bi–O bond distances range from 2.17(2) to 2.44(4) Å. The O–Bi–O bond angles range from 68.7(12)° to 149.9(10)°. The two Se^{4+} cations reveal three-coordinate geometries, in which asymmetric SeO_3 and $SeO_2(OH)$ polyhedra are observed. The Se–O bond lengths range from 1.617(19) to 1.75(3) Å, and the O–Se–O bond angles range from 93.5(18)° to 112.2(18)°. Similar to those of Bi^{3+} cations, the Se^{4+} cations are also in asymmetric coordination environments attributable to the stereoactive lone pair. We found that one of the oxygen atoms connected to Se^{4+} should be an OH group. Bond valence calculations[22] on the oxygen sites exhibit values of 1.97, 2.28, 1.18, 1.71, 2.13, and 1.98 for O(1), O(2), O(3), O(4), O(5), and O(6), respectively, which strongly indicates the hydrogen atom must be linked to the O(3). The result is consistent with the Se–O bond distances: whereas the Se(1)–O(3) bond reveals the longest length of 1.75(3) Å, the remaining Se–O distances for normal selenite groups range from 1.617(19) to 1.71(3) Å. This observation is consistent with those of previously reported materials containing a hydrogen selenite group.[23] The infrared spectrum also supports the presence of a Se–O–H group in the material (see Infrared Spectroscopy section).

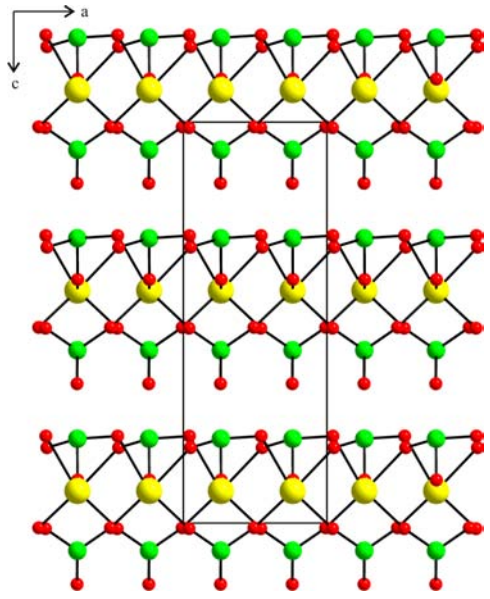

Figure 2. Ball-and-stick representation of $Bi(SeO_3)(HSeO_3)$ in the *ac*-plane. The asymmetric BiO_5 and SeO_3 polyhedra link to form a lamellar structure (green, Se; yellow, Bi; red, O). Hydrogen atoms are omitted for clarity.

As can be seen in Figure 3a, the five-coordinate $Bi(1)O_5$ and the three-coordinate $Se(1)O_2(OH)$ polyhedra share their corners through O(1) and O(2) and form a one-dimensional chain along the [100] direction. Stacks of infinite chains obtained from the corner-sharing of two asymmetric polyhedra, $Bi(1)O_5$ and $Se(1)O_2(OH)$, are observed in the *bc*-plane (see Figure 3b,c). Each chain is further linked by $Se(2)O_3$ polyhedra through O(4), O(5), and O(6) along the approximate [001] direction, and a corrugated layered structure is completed. As seen in Figure 3d, four- and six-membered rings (4MRs and 6MRs) composed of both BiO_5 and SeO_3 polyhedra are observed in the layer. Although the layer topologies are different, a few lamellar structures consisting of only polyhedra of lone pair cations such as Sb^{3+} and/or Te^{4+} have been reported earlier.[24] Interestingly, the 4MRs and the 6MRs in $Bi(SeO_3)(HSeO_3)$ are almost perpendicular to each other. The dimensions of 4MRs and 6MRs are approximately 3.40 Å × 3.62 Å and 2.39 Å × 3.62 Å, respectively, taking into account the ionic radii of selenium and bismuth.[25] In connectivity terms, the structure of $Bi(SeO_3)(HSeO_3)$ can be described as neutral layers of $\{[Bi(1)^{3+}O_{5/2}]^{-2}\ [Se(1)^{4+}O_{2/2}OH]^{+1}[Se(2)^{4+}O_{3/2}]^{+1}\}^0$. Bond valence calculations[22] for the Bi^{3+}, Se^{4+}, and O^{2-} result in values of 2.89, 4.13–4.22, and 1.71–2.28, respectively.

Infrared Spectroscopy. The infrared spectra of $Bi_2(SeO_3)_2(SeO_4)$, $Bi_2(TeO_3)_2(SeO_4)$, and $Bi(SeO_3)(HSeO_3)$ exhibit bands of Bi–O, Se^{4+}–O, Te^{4+}–O, Se^{6+}–O, and OH vibrations. While the bands occurring at around 445–845 and 630–720 cm^{-1} are attributable to the Se^{4+}–O and Te^{4+}–O vibrations, respectively, a characteristic band at 1216 cm^{-1} is ascribed to the Se^{4+}–O bond in hydrogen selenite group. The bands at 1635 and 2370 cm^{-1} strongly suggest the presence of OH group in the material. The Se^{6+}–O vibrations are observed at about 410–860 cm^{-1}. The Bi–O vibrations are overlapped with those of the Se–O bond at about 440–500 and 840 cm^{-1}. The infrared vibrations and assignments are listed in Table 2. The assignments are consistent with those previously reported.[26]

Thermal Analysis. Thermogravimetric analysis (TGA) has been used to investigate the thermal behaviors of the reported materials. $Bi_2(SeO_3)_2(SeO_4)$ and $Bi_2(TeO_3)_2(SeO_4)$ are

dx.doi.org/10.1021/ic4002384 | *Inorg. Chem.* 2013, 52, 4097–4103

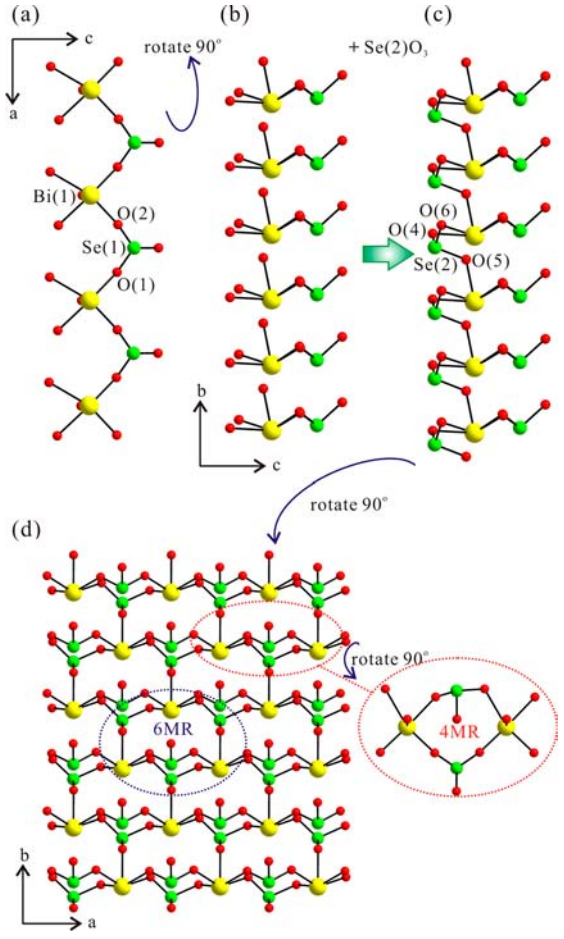

Figure 3. Ball-and stick models of $Bi(SeO_3)(HSeO_3)$ in the *ab*-plane representing (a) chains consisting of corner-shared $Bi(1)O_5$ and $Se(1)O_2(OH)$ polyhedra along the [100] direction, (b) stacks of infinite chains observed in the *bc*-plane, and (c) the linking of $Se(2)O_3$ polyhedra to complete a corrugated layered structure (green, Se; yellow, Bi; red, O). (d) Two interperpendicular four- and six-membered rings composed of BiO_5 and SeO_3 polyhedra are observed within the layer. Hydrogen atoms are omitted for clarity.

Table 2. Infrared Vibrations (cm^{-1}) for $Bi_2(SeO_3)_2(SeO_4)$, $Bi_2(TeO_3)_2(SeO_4)$, and $Bi(SeO_3)(HSeO_3)$

	Bi–O	Se^{4+}–O	Te^{4+}–O	Se^{6+}–O	O–H
$Bi_2(SeO_3)_2(SeO_4)$	505	455		416	
		740		800	
				860	
$Bi_2(TeO_3)_2(SeO_4)$	497		634	412	
			721	802	
				856	
$Bi(SeO_3)(HSeO_3)$	521	445			1631
		751			1269
		1216			

thermally stable up to 450 °C. Above the temperature, both materials start decomposing, attributable to the sublimation of SeO_2. Powder XRD data on the samples measured after heating to 800 °C for $Bi_2(SeO_3)_2(SeO_4)$ and $Bi_2(TeO_3)_2(SeO_4)$ reveal that the materials decomposed to $Bi_{18}SeO_{29}$ (PDF-42–0098) and Bi_2TeO_5 (PDF-38–0420), respectively, along with some unknown materials. With $Bi(SeO_3)(HSeO_3)$, however, thermal decomposition occurs in four steps upon heating. An initial weight loss of 1.12% is observed between 130 and 170 °C, which is attributable to the loss of 0.5 equiv of water (calcd: 0.97%). From 310 to 350 °C, 0.5 equiv of SeO_2 is lost, calcd (exptl): 6.95% (7.97%). Further decomposition attributable to the elimination of one equivalent of SeO_2 occurs between 390 and 510 °C, calcd (exptl): 18.91% (20.12%). The remaining SeO_2 is lost at about 600 °C, which is leaving Bi_2O_3. The TGA plots for all three materials are shown in the Supporting Information.

Second-Order Nonlinear Optical (NLO) Measurements. As $Bi(SeO_3)(HSeO_3)$ crystallizes in a noncentrosymmetric space group, its NLO properties have been investigated. Powder SHG measurements, using 1064 nm radiation, indicate that $Bi(SeO_3)(HSeO_3)$ reveals SHG efficiency of approximately 20 times that of α-SiO_2. By sieving polycrystalline $Bi(SeO_3)(HSeO_3)$ into various particle sizes, ranging from 20 to 150 μm, and measuring the SHG as a function of particle size, the type 1 phase-matching capabilities of the material can be determined. As seen in Figure 4, $Bi(SeO_3)(HSeO_3)$ turns out to be

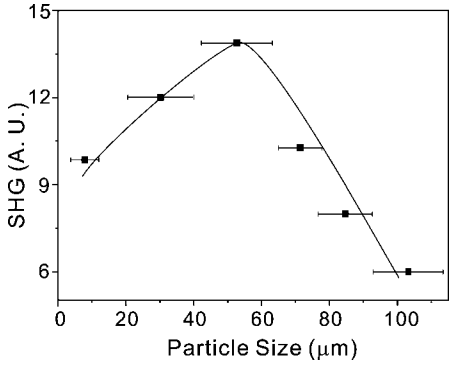

Figure 4. Phase matching curve (type 1) for $Bi(SeO_3)(HSeO_3)$. The curve is to guide the eye and is not a fit to the data.

nonphase-matchable (type 1). Once the SHG efficiency and the phase-matching capability of a material are known, the bulk SHG efficiency, $\langle d_{eff}\rangle_{exp}$, can be estimated.[27] With $Bi(SeO_3)(HSeO_3)$, $\langle d_{eff}\rangle_{exp}$ is calculated to be approximately 2.5 pm V^{-1}.

Structure–Property Relationships. The SHG response of $Bi(SeO_3)(HSeO_3)$ can be explained by analyzing the net polarization arising from individual asymmetric polyhedra. Especially, macroscopic NCS is achieved when local asymmetric coordination units constructively add. In other words, the origin and magnitude of the SHG efficiencies of NCS materials can be understood by determining the "net" direction of the polarizations. In $Bi(SeO_3)(HSeO_3)$, both of the lone pair cations, Bi^{3+} and Se^{4+}, may contribute significantly toward the SHG efficiency attributable to the polarization arising from the asymmetric coordination environment. First, the lone pair on Bi^{3+} points approximately either along the [0–11] or [011] directions. Once taken as a whole, a small moment is observed pointing in the [00–1] direction with Bi^{3+} cation (see Figure 5). Second, each SeO_3 or $SeO_2(OH)$ unit also has a dipole moment attributable to the different charge distribution on Se and O atoms. As seen in Figure 5, the lone pairs on the asymmetric $Se(1)^{4+}$ cations approximately point toward [0–11] or [011] directions. Similar to $Bi(1)^{3+}$ cations, as the local moment for the $Se(1)O_2(OH)$ points in the opposite direction of the lone pair, a small moment in the [00–1] direction attributable to the alignment of lone pairs on $Se(1)^{4+}$ cations is observed. Finally, the lone pairs on the $Se(2)^{4+}$ cations

dx.doi.org/10.1021/ic4002384 | Inorg. Chem. 2013, 52, 4097–4103

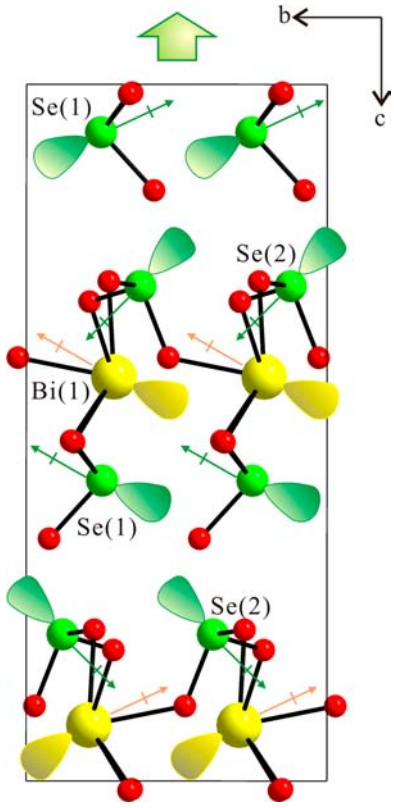

Figure 5. Ball-and-stick representation of $Bi(SeO_3)(HSeO_3)$ in the *bc*-plane (green, Se; yellow, Bi; red, O). A small moment is observed toward the [00−1], [00−1], and [001] directions attributable to the asymmetric $Bi(1)O_5$, $Se(1)O_2(OH)$, and $Se(2)O_3$ groups. Once taken as a whole, a net moment is observed along the [00−1] direction.

approximately point toward [0−1−1] or [01−1] directions. Then a net moment arising from the vector sum of the polarization for $Se(2)O_3$ polyhedra is observed in the [001] direction. Thus, taking the moments as a whole, a net moment for $Bi(SeO_3)(HSeO_3)$ is observed along the [00−1] direction, which is responsible for the observed moderate SHG response, 20 times that of α-SiO_2. The moderate SHG efficiency may be attributed to the lack of greater constructive addition of the dipole moments. Although the local dipole moments for $Bi(1)O_5$ and $Se(1)O_2(OH)$ are aligned in the same direction, those for $Se(2)O_3$ point toward opposite direction, which is detrimental to the SHG efficiency of the material. Besides, on the basis of refined twin ratio, 0.48(4), the crystal itself is twinned.[28] An inversion twinning can also have an effect on the SHG if the domain sizes in a polysynthetic twin are small compared to the wavelength of the light. Although the structural determination was not hindered because the twin operation belongs to the same Laue group of the crystal, any SHG produced by one twin may be weakened by the other.

All three reported materials contain cations in asymmetric coordination environments such as Bi^{3+}, Se^{4+}, and Te^{4+}. In order to better understand the asymmetric coordination environment and the macroscopic net polarization, the local dipole moments for the materials have been calculated, from which the direction and magnitude of the distortions in BiO_5, BiO_6, SeO_3, and TeO_3 polyhedra can be quantified. This method has been used earlier with respect to metal oxy-fluoride octahedra using a bond-valence approach.[29] With the lone pair polyhedra, the lone pair is assigned a charge of −2 and the localized Bi^{3+}, Se^{4+}, and Te^{4+} lone pair distances are estimated to be 0.98, 1.22, and 1.25 Å based on earlier work by Galy and Meunier.[30] Using this methodology, we found that the local dipole moments for the BiO_5, BiO_6, SeO_3, and TeO_3 polyhedra are approximately 10.34, 5.50−6.31, 7.32−11.76, and 10.75 D (D = Debyes), respectively (see Table 3). The values are consistent with those reported values.[31]

Table 3. Summary of the Dipole Moments for BiO_5, BiO_6, SeO_3, and TeO_3 Polyhedra (D = Debyes)

compound	species	dipole moment (D)
$Bi_2(SeO_3)_2(SeO_4)$	$Bi(1)O_6$	5.50
$Bi_2(SeO_3)_2(SeO_4)$	$Se(1)O_3$	7.32
$Bi_2(TeO_3)_2(SeO_4)$	$Bi(1)O_6$	6.31
$Bi_2(TeO_3)_2(SeO_4)$	$Te(1)O_3$	10.75
$Bi(SeO_3)(HSeO_3)$	$Bi(1)O_5$	10.34
$Bi(SeO_3)(HSeO_3)$	$Se(1)O_2(OH)$	11.76
$Bi(SeO_3)(HSeO_3)$	$Se(2)O_3$	8.00

CONCLUSIONS

Pure phases of three new bismuth selenium oxides materials, $Bi_2(SeO_3)_2(SeO_4)$, $Bi_2(TeO_3)_2(SeO_4)$, and $Bi(SeO_3)(HSeO_3)$, have been successfully synthesized by hydrothermal and standard solid-state reactions. The materials were characterized by X-ray diffraction, IR spectroscopy, TGA, and dipole moment calculations. While centrosymmetric three-dimensional structures of $Bi_2(SeO_3)_2(SeO_4)$ and $Bi_2(TeO_3)_2(SeO_4)$ consist of $Bi^{3+}O_6$, $Se^{4+}O_3$ (or $Te^{4+}O_3$), and $Se^{6+}O_4$ polyhedra, non-centrosymmetric $Bi(SeO_3)(HSeO_3)$ is composed of corrugated layers with $Bi^{3+}O_5$ and $Se^{4+}O_3$ polyhedra. Powder SHG measurements on NCS $Bi(SeO_3)(HSeO_3)$, using 1064 nm radiation, indicate that the material is not phase-matchable (type 1) with a SHG efficiency of approximately 20 times that of α-SiO_2. A net moment arising from BiO_5 and SeO_3 groups is responsible for the observed moderate SHG response for $Bi(SeO_3)(HSeO_3)$.

ASSOCIATED CONTENT

Supporting Information

X-ray crystallographic file in CIF format, calculated and observed X-ray diffraction patterns, IR spectra, and thermal analysis diagrams for $Bi_2(SeO_3)_2(SeO_4)$, $Bi_2(TeO_3)_2(SeO_4)$, and $Bi(SeO_3)(HSeO_3)$. This material is available free of charge via the Internet at http://pubs.acs.org.

AUTHOR INFORMATION

Corresponding Author

*E-mail: kmok@cau.ac.kr. Phone: +82-2-820-5197. Fax: +82-2-825-4736.

Author Contributions

†These two authors contributed equally to this work and are co-first-authors.

Notes

The authors declare no competing financial interest.

ACKNOWLEDGMENTS

This research was supported by Basic Science Research Program through the National Research Foundation of Korea (NRF) funded by Ministry of Education, Science & Technology (Grant 2010-0002480).

REFERENCES

(1) (a) Sciau, P.; Lapasset, J.; Moret, J. *Acta Crystallogr., Sect. C* **1986**, *42*, 1688. (b) Thomas, P.; Jeansannetas, B.; Champarnaud-Mesjard, J. C.; Frit, B. *Eur. J. Solid State Inorg. Chem.* **1996**, *33*, 637. (c) Mercurio, D.; Champarnaud-Mesjard, J. C.; Gouby, I.; Frit, B. *Eur. J. Solid State Inorg. Chem.* **1998**, *35*, 49. (d) Ok, K. M.; Bhuvanesh, N. S. P.; Halasyamani, P. S. *Inorg. Chem.* **2001**, *40*, 1978. (e) Oufkir, A.; Dutreilh, M.; Thomas, P.; Champarnaud-Mesjard, J. C.; Marchet, P.; Frit, B. *Mater. Res. Bull.* **2001**, *36*, 693. (f) Porter, Y.; Halasyamani, P. S. *Inorg. Chem.* **2003**, *42*, 205. (g) Charkin, D. O.; Morozov, O. S.; Ul'yanova, E. A.; Berdonosov, P. S.; Dolgikh, V. A.; Dickinson, C.; Wuzong, Z.; Lightfoot, P. *Solid State Sci.* **2006**, *8*, 1029. (h) Kim, M. K.; Jo, V.; Lee, D. W.; Ok, K. M. *Dalton Trans.* **2010**, *39*, 6037. (i) Cao, Z.; Yue, Y.; Yao, J.; Lin, Z.; He, R.; Hu, Z. *Inorg. Chem.* **2011**, *50*, 12818. (j) Nguyen, S. D.; Yeon, J.; Kim, S.-H.; Halasyamani, P. S. *J. Am. Chem. Soc.* **2011**, *133*, 12422.

(2) (a) Wickleder, M. S. *Chem. Rev.* **2002**, *102*, 2011. (b) Ok, K. M.; Halasyamani, P. S. *Angew. Chem., Int. Ed.* **2004**, *43*, 5489.

(3) (a) Semenova, T. F.; Rozhdestvenskaya, I. V.; Filatov, S. K.; Vergasova, L. P. *Miner. Mag.* **1992**, *56*, 241. (b) Johnsson, M.; Tornroos, K. W.; Mila, F.; Millet, P. *Chem. Mater.* **2000**, *12*, 2853. (c) Millet, P.; Bastide, B.; Pashchenko, V.; Gnatchenko, S.; Gapon, V.; Ksari, Y.; Stepanov, A. *J. Mater. Chem.* **2001**, *11*, 1152. (d) Millet, P.; Johnsson, M.; Pashchenko, V.; Ksari, Y.; Stepanov, A.; Mila, F. *Solid State Ionics* **2001**, *141*, 559. (e) Becker, R.; Johnsson, M.; Kremer, R. K.; Lemmens, P. *Solid State Sci.* **2003**, *5*, 1411. (f) Mayerová, Z.; Johnsson, M.; Lidin, S. *J. Solid State Chem.* **2005**, *178*, 3471. (g) Mayerová, Z.; Johnsson, M.; Lidin, S. *Angew. Chem., Int. Ed.* **2006**, *45*, 5602.

(4) (a) Jona, F.; Shirane, G. *Ferroelectric Crystals*; Pergamon Press: Oxford, U.K., 1962. (b) Cady, W. G. *Piezoelectricity; An Introduction to the Theory and Applications of Electromechanical Phenomena in Crystals*; Dover: New York, 1964. (c) Lang, S. B. *Sourcebook of Pyroelectricity*; Gordon & Breach Science: London, 1974. (d) *Principles and Applications of Ferroelectrics and Related Materials*; Lines, M. E., Glass, A. M., Eds.; Oxford University Press: Oxford, U.K., 1991.

(5) (a) Gillespie, R. J.; Nyholm, R. S. *Q. Rev., Chem. Soc.* **1957**, *11*, 339. (b) Orgel, L. E. *J. Chem. Soc.* **1959**, 3815. (c) Seshadri, R.; Hill, N. A. *Chem. Mater.* **2001**, *13*, 2892.

(6) (a) Opik, U.; Pryce, M. H. L. *Proc. R. Soc. London* **1957**, *A238*, 425. (b) Bader, R. F. W. *Mol. Phys.* **1960**, *3*, 137. (c) Bader, R. F. W. *Can. J. Chem.* **1962**, *40*, 1164. (d) Pearson, R. G. *THEOCHEM* **1983**, *103*, 25. (e) Wheeler, R. A.; Whangbo, M.-H.; Hughbanks, T.; Hoffmann, R.; Burdett, J. K.; Albright, T. A. *J. Am. Chem. Soc.* **1986**, *108*, 2222.

(7) (a) Nikol, H.; Vogler, A. *J. Am. Chem. Soc.* **1991**, *113*, 8988. (b) Nikol, H.; Vogler, A. *Inorg. Chem.* **1993**, *32*, 1072. (c) Watson, G. W.; Parker, S. C. *J. Phys. Chem. B* **1999**, *103*, 1258. (d) Watson, G. W.; Parker, S. C.; Kresse, G. *Phys. Rev. B* **1999**, *59*, 8481.

(8) Effenberger, H. *Acta Chem. Scand.* **1996**, *50*, 967.

(9) Effenberger, H. *J. Alloys Compd.* **1998**, *281*, 152.

(10) Rademacher, O.; Goebel, H.; Oppermann, H. *Z. Kristallogr.—New Cryst. Struct.* **2000**, *215*, 339.

(11) Rademacher, O.; Goebel, H.; Ruck, M.; Oppermann, H. *Z. Kristallogr.—New Cryst. Struct.* **2001**, *216*, 29.

(12) Li, P. X.; Kong, F.; Hu, C.; Zhao, N.; Mao, J. G. *Inorg. Chem.* **2010**, *49*, 5943.

(13) Effenberger, H. *Mineral. Petrol.* **1987**, *36*, 3.

(14) (a) Giester, G. *Monatsh. Chem.* **1989**, *120*, 661. (b) Baran, J.; Lis, T.; Marchewka, M.; Ratajczak, H. *J. Mol. Struct.* **1991**, *250*, 13. (c) Giester, G. *Monatsh. Chem.* **1992**, *123*, 957. (d) Morris, R. E.; Wilkinson, A. P.; Cheetham, A. K. *Inorg. Chem.* **1992**, *31*, 4774. (e) Harrison, W. T. A.; Zhang, Z. *Eur. J. Solid State Inorg. Chem.* **1997**, *34*, 599. (f) Krugermann, I.; Wickleder, M. S. *Z. Anorg. Allg. Chem.* **2002**, *628*, 147. (g) Weil, M.; Kolitsch, U. *Acta Crystallogr.* **2002**, *C58*, 47. (h) Wickleder, M. S.; Buchner, O.; Wickleder, C.; Sheik, S. e.; Brunklaus, G.; Eckert, H. *Inorg. Chem.* **2004**, *43*, 5860.

(15) *SAINT Program for Area Detector Absorption Correction*, version 4.05; Siemens Analytical X-ray Instruments: Madison, WI, 1995.

(16) Blessing, R. H. *Acta Crystallogr.* **1995**, *A51*, 33.

(17) (a) Sheldrick, G. M. *SHELXS-97—A Program for Automatic Solution of Crystal Structures*; University of Goettingen: Goettingen, Germany, 1997. (b) Sheldrick, G. M. *SHELXL-97—A Program for Crystal Structure Refinement*; University of Goettingen: Goettingen, Germany, 1997.

(18) Farrugia, L. J. *J. Appl. Crystallogr.* **1999**, *32*, 837.

(19) Kurtz, S. K.; Perry, T. T. *J. Appl. Phys.* **1968**, *39*, 3798.

(20) Ok, K. M.; Chi, E. O.; Halasyamani, P. S. *Chem. Soc. Rev.* **2006**, *35*, 710.

(21) Housecroft, C. E.; Sharpe, A. G. *Inorganic Chemistry*, 2nd ed.; Pearson: Essex, U.K., 2005.

(22) (a) Brown, I. D.; Altermatt, D. *Acta Crystallogr.* **1985**, *B41*, 244. (b) Brese, N. E.; O'Keeffe, M. *Acta Crystallogr.* **1991**, *B47*, 192.

(23) (a) Morris, R.; Harrison, W. T. A.; Stucky, G. D.; Cheetham, A. K. *Acta Crystallogr., Sect. C* **1992**, *48*, 1182. (b) Castro, A.; Enjalbert, R.; Pedro, M. d.; Trombe, J. C. *J. Solid State Chem.* **1994**, *112*, 418. (c) Harrison, W. T. A. *Acta Crystallogr., Sect. E* **2006**, *62*, i152. (d) Burns, W. L.; Ibers, J. A. *J. Solid State Chem.* **2009**, *182*, 1457.

(24) (a) Alonso, J. A. *J. Chem. Soc., Dalton Trans.* **1998**, 1947. (b) Jo, V.; Kim, M. K.; Lee, D. W.; Shim, I.-W.; Ok, K. M. *Inorg. Chem.* **2010**, *49*, 2990.

(25) Shannon, R. D. *Acta Crystallogr.* **1976**, *A32*, 751.

(26) (a) Baran, J.; Marchewka, M. K.; Ratajczak, H. *J. Mol. Struct.* **1997**, *436–437*, 257. (b) Yu, J.; Xiong, J.; Cheng, B.; Yu, Y.; Wang, J. *J. Solid State Chem.* **2005**, *178*, 1968. (c) Zhang, S.-Y.; Hu, C.-L.; Sun, C.-F.; Mao, J.-G. *Inorg. Chem.* **2010**, *49*, 11627.

(27) Goodey, J.; Broussard, J.; Halasyamani, P. S. *Chem. Mater.* **2002**, *14*, 3174.

(28) (a) Catti, M.; Ferraris, G. *Acta Crystallogr., Sect. A* **1976**, *32*, 163. (b) Flack, H. D. *Acta Crystallogr., Sect. A* **1983**, *39*, 876.

(29) (a) Maggard, P. A.; Nault, T. S.; Stern, C. L.; Poeppelmeier, K. R. *J. Solid State Chem.* **2003**, *175*, 27. (b) Izumi, H. K.; Kirsch, J. E.; Stern, C. L.; Poeppelmeier, K. R. *Inorg. Chem.* **2005**, *44*, 884.

(30) Galy, J.; Meunier, G. *J. Solid State Chem.* **1975**, *13*, 142.

(31) (a) Ok, K. M.; Halasyamani, P. S. *Inorg. Chem.* **2005**, *44*, 3919. (b) Lee, D. W.; Ok, K. M. *Solid State Sci.* **2010**, *12*, 2036. (c) Lee, D. W.; Oh, S.-J.; Halasyamani, P. S.; Ok, K. M. *Inorg. Chem.* **2011**, *50*, 4473. (d) Lee, D. W.; Kim, S. B.; Ok, K. M. *Inorg. Chem.* **2012**, *51*, 8530. (e) Oh, S.-J.; Lee, D. W.; Ok, K. M. *Inorg. Chem.* **2012**, *51*, 5393. (f) Oh, S.-J.; Lee, D. W.; Ok, K. M. *Dalton Trans.* **2012**, *41*, 2995. (g) Oh, S.-J.; Shin, Y.; Tran, T. T.; Lee, D. W.; Yoon, A.; Halasyamani, P. S.; Ok, K. M. *Inorg. Chem.* **2012**, *51*, 10402.